Study of damage in binary $Fe_{85}Cr_{15}$ alloys irradiated by ions and the effect of an external magnetic field during irradiation

I. García-Cortés [a, *], T. Leguey [b], F.J. Sánchez [a], A. Maira [c], A. Moroño [a], P. Muñoz [a], M. Scepanovic [b], J.F. Marco [d]

[a] Laboratorio Nacional de Fusión, CIEMAT, Av. Complutense 40, 28040 Madrid, Spain
[b] Departamento de Física, Universidad Carlos III de Madrid, Avenida Universidad 30, 28911 Leganés, Madrid, Spain
[c] Centro de Microanálisis de Materiales, Universidad Autónoma de Madrid, Faraday 3, 28049 Madrid, Spain
[d] Instituto de Química Física "Rocasolano", CSIC, Calle de Serrano, 119, 28006 Madrid, Spain

HIGHLIGHTS

- Irradiations by light and self ions reveal significant differences in the Cr and/or vacancies distribution in the alloy.
- Samples irradiated by self-ions show large concentration of vacancy-type defects.
- The external magnetic field can be a non-negligible parameter in the material damage due to ion irradiation.

ARTICLE INFO

ABSTRACT

Understanding radiation-induced damage in iron-chromium alloys is critical for the use of advanced steels in future fusion reactors. However, the role of the strong magnetic fields present in such magnetically confined plasma devices on material damage, though considered important, has not been thoroughly explored to date. In this work, irradiation experiments of $Fe_{85}Cr_{15}$ alloy (15% Cr content) by heavy (Fe^+) and light (He^+) ions have been carried out in order to characterize the damage and, additionally, the influence of an external magnetic field ($B = 0.4$ T) has been taken into account. The analysis of the data has been done with different techniques, the distribution of the Cr and/or vacancies around probe nuclei has been explored by Mössbauer spectroscopy and the vacancy profile by Slow Positron Annihilation Spectroscopy (SPAS). Comparison between samples irradiated by He^+ and Fe^+, in absence of B, reveals significant differences in the average hyperfine magnetic field $(<\Delta H> = 0.8$ T$)$. This can be attributed to changes in the local environment around the probe nuclei (^{57}Fe) where either vacancies or the Cr distribution play a role. From depth-profiling by SPAS in Fe^+ irradiated samples, a large concentration of vacancy-type defects is found with a profile that extends deeper than that predicted by computer simulations. Furthermore, sequential irradiation by Fe^+ and He^+ ions indicates that the He atoms tend to fill the vacancy clusters just in the depth where the He^+ is implanted. On the other hand, small but significant differences in vacancy-type defect profiles are found between the samples irradiated both in the presence and absence of a magnetic field ($B = 0.4$ T) both independently of single and sequential irradiation. Detailed Mössbauer spectroscopy and SPAS analysis seem to point out that external magnetic fields could be a non-negligible parameter in the material damage due to ion irradiation.

© 2019 Elsevier B.V. All rights reserved.

1. Introduction

The selection and design of materials that can withstand the extreme conditions of a fusion power plant have been described as one of the great material science challenges [1]. The high particle flux, high thermal load, thermal mechanical stresses and the production of transmutation elements combine to produce a uniquely hostile environment. High-chromium ferritic/martensitic steels are strong candidates as structural materials for these fusion devices. One reason for selecting these steels is their superior resistance to irradiation, in terms of low damage accumulation and relatively

low swelling [2–4]. The determination of the precise Cr percentage to be used for the Fe-Cr alloys in structural materials is still an open question. For instance, if it is high (more than about 10%) Cr is beneficial because it prevents oxidation. However, above a threshold of [Cr] > 8–9%, the formation of Cr rich alpha prime phase can result in the embrittlement of the material [5–7]. Moreover, the large amount of helium produced in neutron-irradiated metals as a result of transmutation reactions plays a significant role both in microstructure evolution and mechanical properties degradation [8,9]. Hence, understanding the fundamental behaviour of helium in Fe-Cr alloys is one of the unresolved issues in steel characterization.

To date, most of the studies on these structural materials have been focused on material behaviour as a function of irradiation dose, particle energy, sample temperature, etc. [10]. However, next step fusion devices, such as the International Thermonuclear Experimental Reactor (ITER) [11] and Demonstration Power Plant (DEMO) [12], are magnetically confined devices and the performance of the materials under reactor conditions when high magnetic fields are present is still unexplored. Besides, theoretical predictions suggest that magnetism can be a non-negligible factor in defining the defect properties induced by He irradiation or in determining the atomic distribution in Fe-Cr alloys [13,14]. Material micro-structural properties can be modified by defect propagation due to irradiation. It is considered that such propagation may be affected by external magnetic fields, as recently pointed in Ref. [15]. For this reason, more detailed experimental knowledge of structural materials is sought, in particular with regard to mobility and clustering, as well as helium and hydrogen accumulation in reactor conditions.

From the experimental point of view, it is necessary to study the behaviour of Fe-Cr alloys under irradiation by 14 MeV neutrons. The ability to simulate the whole neutron-induced damage effects and its main consequences on both microstructure and mechanical properties changes in nuclear materials by ion beams was first analyzed by Averback [16] and Ullmaier [17]. In this way, such damage is usually simulated by heavy ions (mainly self-ions) while transmutation products (H and He) are simulated by irradiation with light ions (H and He) [18]. As the 14 MeV neutrons penetrate the material they lose energy primarily by knock-ons of Fe atoms, these latter atoms having a range of energies with a maximum around 1 MeV. Thus, the main damage arising from neutron irradiation is due to these energetic Fe atoms which, in turn, create a cascade of radiation damage. In the experiments reported here, cascade damage is induced by a beam of self-ions (Fe^+) at 1 MeV. Moreover, the transmutation products are simulated by He^+ ions at 45 keV in order to ensure that He is located into the same region pre-damage by Fe^+ ions. Then the energies were specifically chosen to achieve the maximum damage at same depths for both ions, considering the limitations in energy of the CIEMAT implanter, where a part of the experiments was performed.

In this paper, experimental results for a series of $Fe_{85}Cr_{15}$ specimens irradiated with Fe^+ and He^+ ions, in single and sequential form are presented. Every irradiation was carried out in pairs of samples, *i.e.* with and without the effect of an external magnetic field. This is done in order to understand the behaviour of the structural material under fusion reactor conditions, where strong magnetic fields are present. The characterization of damage has been performed using Mössbauer Spectroscopy to understand the Cr and vacancies distribution around the iron atoms in the alloy and Slow Positron Annihilation Spectroscopy to study the profile of vacancy-type defects.

2. Experimental procedure

2.1. Specimens

The samples investigated in this paper were prepared from EFDA/EURATOM model Fe-Cr alloys with 15%Cr ($Fe_{85}Cr_{15}$). Here Fe_{85} and Cr_{15} are shorthand for $Fe_{84.85}Cr_{15.15}$, respectively. According to the EFDA Armines report [19], the alloy contain a few impurities in very minor concentrations (see Table 1).

This material was delivered in the form of bars, 10.9 mm in diameter, in a re-crystalized state after cold reduction of 70% and then heat treated for 1 h under pure argon flow, at temperatures of 850 °C, followed by air cooling. For these experiments, 1 mm thick slices were cut from each bar by spark erosion and thinned by grinding and polishing on a plane-parallel polishing machine to a final thickness about 300 μm each.

2.2. Irradiation conditions

$Fe_{85}Cr_{15}$ specimens were irradiated in pairs for each experiment. This involved one sample being irradiated in the presence of an external magnetic field, B, at 0.4 T, and the other in the absence of B. A dedicated custom sample holder with a permanent magnet embedded behind one of the samples was used. In this sytem, the magnetic field lines are oriented normal to the sample surface in order to avoid ion beam spreading, see Ref. [15] for a more detailed explanation of the experimental system. Table 2 collects the list of samples together with their irradiation conditions in the case of single irradiation while Table 3 collets the details of sequential irradiation conditions.

Theoretical damage profiles for the samples were calculated using the SRIM code [20]. Fig. 1a shows the vacancy profile for He^+ @ 45 keV while Fig. 1b shows the damage simulated by Fe^+ @ 1 MeV.

Three irradiation types were carried out at the following irradiation facilities:

2.2.1. CMAM

A set of samples was irradiated at the Centre for Micro Analysis of Materials (CMAM) in Madrid, Spain [21] with a sampler holder connected to a cold finger [15]. The irradiations were carried out with Fe^+ @ 1 MeV up to a damage of 22 dpa (24 nA, $1.1 \, 10^{-3}$ dpa/s) and 30 dpa (65 nA, $2.7 \, 10^{-3}$ dpa/s). The Bragg peak was estimated at ~300 nm from the sample surface, see Fig. 1a. The samples were irradiated at a temperature of −80 °C to avoid possible temperature-related recovery of defects during irradiation. The temperature was monitored with thermocouples type K and it remained stable during the irradiation.

2.2.2. CIEMAT implanter

Another set of samples was irradiated with He^+ @ 45 keV using the ion accelerator at CIEMAT (Madrid, Spain) with a current of 150-200 nA. This facility is a 60 keV Danfysik ion implanter (beam current up to 150 μA) that permits ion implantation with helium, hydrogen and deuterium ions among others. It is mainly dedicated

Table 1
Concentration of residual contaminants on EFDA Fe-Cr (1%Cr wt) samples used in this work.

Alloy	C wt ppm	S wt ppm	O wt ppm	N wt ppm	P wt ppm
Fe 1% Cr	4/5	6/7	4/4	5/5	<10

Table 2
Single irradiation. Samples and their irradiation conditions. A.R. means samples un-irradiated, "wo_B" samples irradiated in absence of B and "w_B" irradiated in the presence of B.

$Fe_{85}Cr_{15}$	Ion @ energy	Dose rate (ions/cm$^2 \cdot$ s)	Fluence (ions/cm^2)	Max. dose (dpa) or concentra. (appm)	Max depth (nm)	B
#0/A.R.	A.R.					
#1/He$^+$ wo_B	He$^+$ @45 keV	$7.9 \cdot 10^{12}$	$4\ 10^{16}$	$3.2 \cdot 10^4$ appm	164	No
#2/He$^+$ w_B	He$^+$ @45 keV	$7.9 \cdot 10^{12}$	$4\ 10^{16}$	$3.2 \cdot 10^4$ appm	164	Yes
#3/Fe$^+$ wo_B	Fe+ @ 1 MeV	$4.5 \cdot 10^{11}$	$8.24 \cdot 10^{15}$	22 dpa	357	No
#4/Fe$^+$ w_B	Fe+ @ 1 MeV	$4.5 \cdot 10^{11}$	$8.24 \cdot 10^{15}$	22 dpa	357	Yes
#5/Fe$^+$ wo_B	Fe+ @ 1 MeV	$1.0 \cdot 10^{12}$	$1.12 \cdot 10^{16}$	30 dpa	357	No
#6/Fe$^+$ w_B	Fe+ @ 1 MeV	$1.0 \cdot 10^{12}$	$1.12 \cdot 10^{16}$	30 dpa	357	Yes

Table 3
Sequential irradiation Fe$^+$ (CMAM) and He$^+$ (CIEMAT). "wo_B″ samples irradiated in absence of B and "w_B" irradiated in the presence of B.

$Fe_{85}Cr_{15}$	Fe$^+$ @1 MeV	He$^+$ @ 45 keV	Concentration (appm)	B
#7/seq. wo_B	#3	1.10^{16} (ions/cm^2)	8000	No
#8/seq. w_B	#4	1.10^{16} (ions/cm^2)	8000	Yes

to fusion related research studies [22]. The samples were irradiated at RT. The sample holder was cooled by a water circuit to maintain a controlled temperature during irradiation.

A third set of samples was subjected to a sequential irradiation experiment first using Fe$^+$ @ 1 MeV at the CMAM ion accelerator followed by subsequent irradiation with He$^+$ ions @ 45 keV in the CIEMAT implanter with the same current conditions described above for the irradiations performed in each facility. The energies were specifically chosen to achieve the maximum damage at same depths for both ions, considering the limitations in energy of the CIEMAT implanter. Fig. 1b displays the SRIM profile for these irradiations.

2.3. Analysis techniques

2.3.1. Mössbauer Spectroscopy
Since Mössbauer Spectroscopy has been successfully used to

understand damage in Fe-Cr alloys [23−26] Mössbauer data were recorded from the irradiated materials (samples #1-2 and #5-6 in Table 2) to gain insight on the effect of irradiation. As the experiments for samples had an implantation depth less than one μm, Mössbauer spectra were collected at room temperature by recording conversion electrons in backscattering geometry (CEMS) using a ^{57}Co(Rh) source, a constant acceleration spectrometer and a parallel plate avalanche counter [27]. The velocity scale was calibrated using a 6 μm natural iron foil. All the spectra were computer-fitted and the Mössbauer parameters calculated following the same procedure used in previous studies [24−26].

2.3.2. Slow Positron Annihilation Spectroscopy
Slow Positron Annihilation Spectroscopy (SPAS) was used to characterize the open volume lattice defects generated in the samples irradiated with Fe$^+$ ions at −80 °C up to 22 dpa (samples #3 and #4 in Table 2) and sequentially irradiated by Fe$^+$ and He$^+$ (samples #7 and #8 in Table 3). These samples, together with a reference (non-irradiated) one, were measured by Doppler Broadening (DB) and Coincident Doppler Broadening (CDB) spectroscopy using the variable low-energy positron beam at NEPOMUC (FRM II, Heinz Maier-Leibnitz Zentrum (MLZ), Garching, Germany) [28,29]. The positron implantation energies ranged between 0.2 keV and 30 keV, which corresponds to mean positron implantation depths up to ~1.2 μm in $Fe_{85}Cr_{15}$ and the positron beam diameter varied between 0.3 mm and 3 mm. High-purity germanium radiation
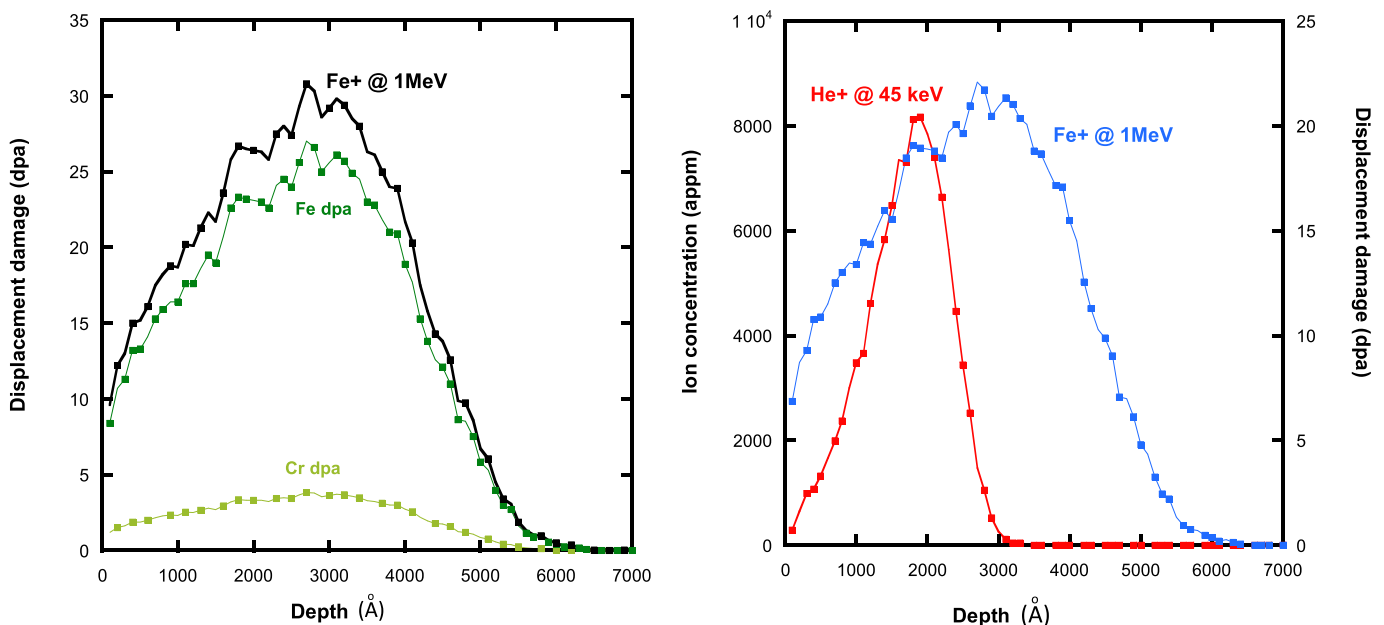

Fig. 1. SRIM profiles for a) left figure: CMAM irradiation, 30 dpa Fe$^+$ ions damage profile and b) right figure: sequential irradiation Fe$^+$ (CMAM) and He$^+$ (CIEMAT).

detectors were used to record the annihilation photo-peak at different positron implantation energies up to 30 keV. The energy resolution of the detectors used was 1.4 keV at 511 keV with a count rate of ~2500 s^{-1}. The Doppler broadening of the 511 keV annihilation line contains information of the electron momentum distribution at the positron annihilation site. In open volume defects the probability of annihilation of core electrons decreases, therefore a narrowing of the annihilation line is observed. DB is characterized using the S and W line shape parameters. The S parameter is calculated as the ratio of counts in the central area of the annihilation peak and the total peak counts, while the W parameter is calculated as the fraction of counts in the high-momentum region.

CDB spectra were recorded in the bulk at incident positron energy of 17 keV. The high momentum spectra contain counts related to the positron annihilation events with core electrons. This signal can be used to obtain information on the chemical species surrounding an annihilation site [30]. The CDB measurements were carried out using two HP Ge detectors in coincidence, placed face to face and separated by 50 cm with the sample centred between the detectors. In order to compare the CDB measurements, the spectra were normalized and the intensity at a given photon energy was divided by the corresponding counts in the CDB spectrum of a reference sample. Pure annealed Fe was used as a reference sample.

3. Results

3.1. Mössbauer analysis results

All the Mössbauer spectra were fitted using the same procedure used in previous studies [15,25], *i.e.,* assuming that only Cr atoms situated within the first (1NN) and second (2NN) neighbour-shells cause measurable changes in the Mössbauer parameters, namely the hyperfine field, *H*, and the isomer shift, *IS*. In this model, the changes both in *H* and *IS* are additive, *i.e.* $X(m, n; x) = X(0, 0; x) - m \Delta X1 - n \Delta X2$, where $X = H$ or IS, $\Delta X1$ and $\Delta X2$ stand for the change in X due to the presence of one Cr atom in 1NN and one Cr atom in 2NN, respectively, around an iron atom, m and n are the number of Cr atoms in 1NN and 2NN, respectively, and x refers to the Cr concentration. Given the composition of the present samples, their spectra were fitted using a superposition of 14 sextets with different hyperfine parameters, this depending on the number of neighbours for the iron atoms. Taking into account this additive rule, the analysis starts with values $H(0,0) = 34.1$ T, $IS(0,0) = 0.00$ mms^{-1}, $\Delta H1 = -3.1$ T, $\Delta H2 = -2.0$ T, $\Delta IS1 = -0.022$ mms^{-1} and $\Delta IS2 = -0.009$ mms^{-1}. These values are close to those obtained previously for a Fe-Cr alloys of similar composition [25,31]. Next, in order to avoid divergences in the fit, all the spectra were fitted using the same line width, for the individual sextets. As an example, Fig. 2a shows the Mössbauer spectra corresponding to three of the samples listed in Table 2: sample #0, specimen a received (A.R.), sample #1, sample irradiated by light ions (He$^+$) and sample #5, irradiated by heavy ions (Fe$^+$) to 30 dpa, all in the absence of an external magnetic field. The spectra of the samples irradiated in the presence of an external magnetic field were fitted using an identical procedure, as seen in Fig. 2b. In addition to these sextets all the spectra show the presence of a small (less than 7% of the spectral area) central paramagnetic doublet with Mössbauer parameters ($QS = 0.31$-0.40 mms^{-1}; $IS = 0.75$-0.95 mms^{-1}), characteristic of high spin Fe^{3+} in distorted oxygen octahedral coordination. These doublets can arise most likely from the presence of a thin oxidation layer formed after exposure of a specimen to the laboratory atmosphere [32] since their corresponding hyperfine parameters are characteristic of amorphous or super-paramagnetic Fe^{3+} oxyhydroxides [33]. Given the large positive magnitude of the isomer shift of this doublet, its assignment to paramagnetic impurities dissolved in the iron matrix can be ruled out.
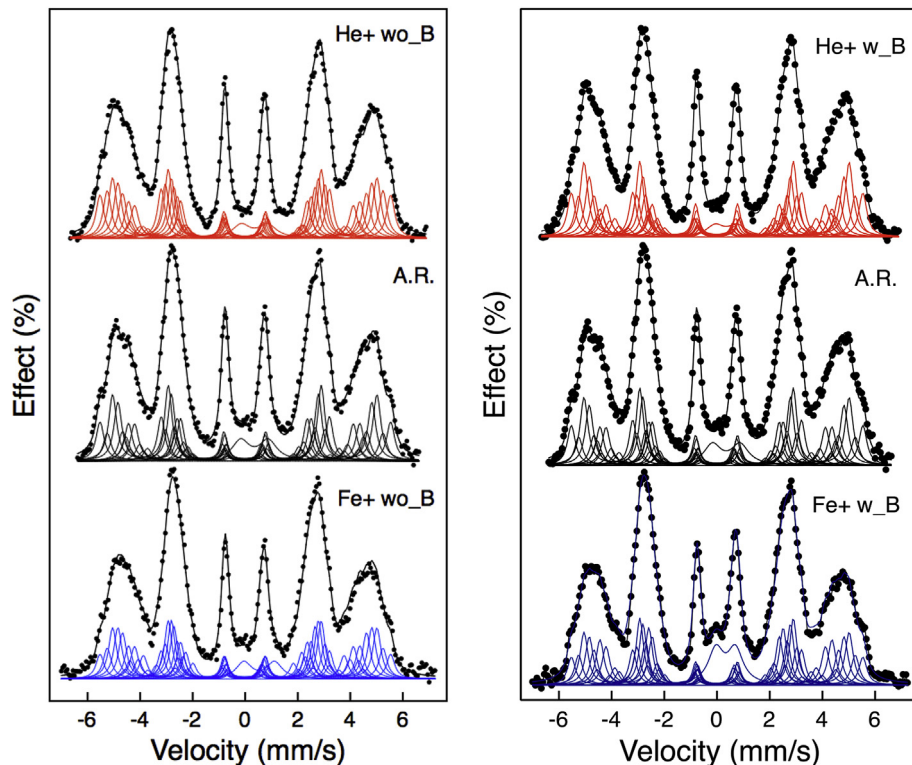

Fig. 2. Left a) and Right b). Fitted Mössbauer spectra for Fe$_{85}$Cr$_{15}$: irradiated by He$^+$ (samples #1,2, top), as received (centre, sample #0) and Fe$^+$ (bottom, samples #5,6). 2a) in the absence of an external magnetic field (wo_B). 2b) in the presence of an external magnetic field (w_B). The coloured peaks are 14 sextets showing different Cr neighbouring groups (see text for explanation).
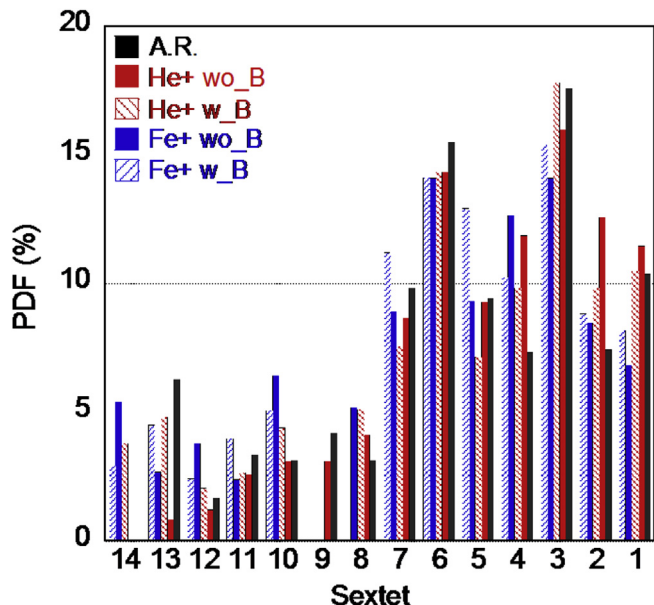
Fig. 3. Probability Density Function (PDF) of sextet relative areas obtained from the fit of the samples A.R., irradiated by He^+ and Fe^+ both in absence (wo_B) and presence of B field (w_B). Samples #1-2 and #5-6.

Fig. 4. Average hyperfine field <H> for the $Fe_{85}Cr_{15}$ samples irradiated under different conditions (blue points are samples irradiated by Fe^+ and red squares irradiated by He^+). Error bars are about 0.1 T. Note that in X-axis: "A.R." means samples un-irradiated, "wo_B" samples irradiated in absence of B and "w_B" irradiated in the presence of B. (For interpretation of the references to colour in this figure legend, the reader is referred to the Web version of this article.)

Inspection of Fig. 2 indicates that the profile distribution of the various sextets in these samples, which is related to the distribution of the possible different atomic configurations around the iron atoms, changes with the type of ion used for irradiation. Fig. 3 collects the relative areas of the different sextets used to fit the spectra shown in Fig. 2a plus those used to fit the spectra of the samples irradiated under a magnetic field (Fig. 2b). The results indicate that the application of such a field also changes the profile of the sextet distributions and, therefore, different atomic configurations can be expected.

Given the large number of sextets present in the distributions it is difficult to follow the individual variations for each atomic configuration in each sample. A parameter that can be quite informative is the average hyperfine magnetic field, <H>, which is calculated as the weighted average of the hyperfine fields associated with particular atomic configurations, using the same procedure as in Refs. [15,25]. Variations in <H> are considered to arise from a combined effect of the vacancies generated during irradiation and the degree of Cr ordering in the alloy, *i.e.* if Cr distributes in isolated clusters due to irradiation, <H> would increase, while short-range-order (SRO) and vacancies would decrease this magnitude [24—26].

The variation in the magnitude of <H> brought about by He^+ and Fe^+ irradiation, both with and without the application of an external field, is presented in Fig. 4. It can be observed that in the specimens irradiated with He^+, <H> increases with respect to the A.R. sample both in the absence and in the presence of a B field. On the contrary, the specimens irradiated with heavier Fe^+ ions present a decrease in the <H> magnitude in both cases. As compared with the A.R. sample, the sample irradiated with He^+ in the absence of B produces the largest variations in terms of <H>. It seems that the variations observed in <H> with respect to the A.R. are smaller when a magnetic field is present.

The second effect of these irradiation experiments can be observed from the distribution of Fe/Cr atoms described in terms of the SRO parameters, α_i, as deduced from the Mössbauer spectroscopic data. As outlined elsewhere [24 and references therein], the SRO parameters can be defined locally, *i.e.* for a given (*m, n*) or its
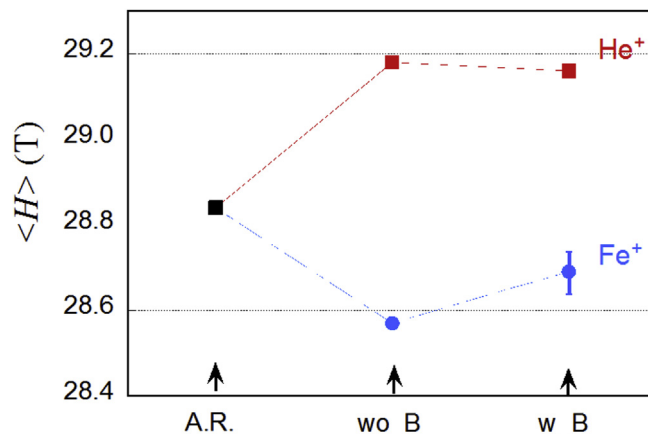
average for a particular neighbour shell: for 1NN, $<\alpha_1>$, for 2NN, $<\alpha_2>$, for 1NN-2NN, $<\alpha_{12}>$. This magnitude is calculated according to $<\alpha_{12}> = 1 - <m+n>/0.14x$, where $<m+n>$ is the average number of Cr atoms in *1NN-2NN*, determined from the Mössbauer spectra. We would like to point out that this model only takes into account the presence of Cr and Fe atoms around the probe nuclei but not considers any vacancies or the presence of any other light elements that can influence the final value of the SRO parameters. The results for samples #0-2 and #5-6 are shown in Table 4.

First, as seen in Table 4, most SRO $<\alpha_i>$ parameters are different from zero. This indicates that the distribution of Fe/Cr atoms is not random in the majority of the cases. Now, concerning the 1NN-shell, $<\alpha_1>$, all the values are positive. Next, for the 2NN-shell the $<\alpha_2>$ values are all negative. Moreover, $<\alpha_{12}>$ values depend of the type of damage. See Fig. 5 which shows values of $<\alpha_{12}>$ versus $<m+n>$. With the same model, when $<\alpha_{12}>$ is close to zero then Cr atoms are randomly distributed over the first two shells, *1NN-2NN*. Here for positive values of $<\alpha_{12}>$ (samples irradiated by He^+) the distribution of Cr atoms indicates clustering, a process that is less effective if the sample is irradiated in the presence of a B field. In contrast, a negative value of $<\alpha_{12}>$ is indicative of a more ordered distribution of Cr atoms, as is the case of the samples irradiated by Fe^+. A representative error bar is shown in the same figure. Thus some care must be taken in the above interpretations.

Finally, comparing comparing the wo_B and w_B data in Table 4, it is possible to highlight the influence of the impacting ion on the SRO parameters. Hence, Fig. 6 shows the relative changes between the measured $<\alpha_1>$ and $<\alpha_2>$ for each irradiated case and the A.R. sample. The effect of ion irradiation is clearly different depending on the ion used for damage (He^+ or Fe^+) and on the characteristics

Table 4
Principal Mössbauer Spectroscopy analysis parameters. "wo_B" samples irradiated in absence of B and "w_B" irradiated in the presence of B.

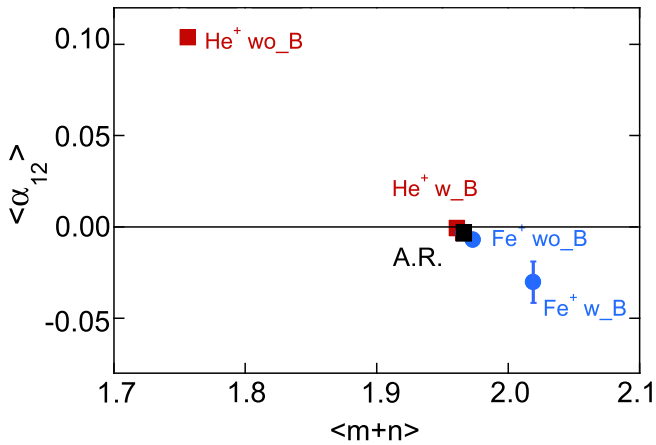| #Sample	B	H(0,0)	<H>	$<\alpha_1>$	$<\alpha_2>$	$<\alpha_{1,2}>$	A2/A3	$<m+n>$
#0/A.R.		34.3	28.8	0.24	−0.32	0.00	3.2	1.97
#1/He^+ wo_B	No	34.3	29.2	0.25	−0.08	0.10	3.2	1.76
#2/He^+ w_B	Yes	34.3	29.2	0.20	−0.26	0.00	2.8	1.96
#5/Fe^+ wo_B	No	34.3	28.6	0.19	−0.27	−0.01	3.2	1.97
#6/Fe^+ w_B	Yes	34.3	28.7	0.08	−0.18	−0.03	3.5	2.02

Fig. 5. Dependence of the SRO parameter, α_{12}, on the irradiation conditions (see legend for each point) and on the distribution of Cr into the two first shells. Note: "A.R." means samples un-irradiated, "wo_B″ samples irradiated in absence of B and "w_B" irradiated in the presence of B.

of the neighbor shell. This is an important consideration for theoretical calculations or modelling.

3.2. Slow positron annihilation results

Fig. 7 shows the S and W parameters obtained as a function of incident positron energy for the samples irradiated with Fe^+ ions up to 22 dpa in the absence or presence of magnetic field (samples # 3 and #4), and for the samples sequentially irradiated with Fe^+ ions (22 dpa) and He^+ ions up to 8000 appm (samples #7 and #8), together with the values measured for the non-irradiated $Fe_{85}Cr_{15}$ alloy and well-annealed pure Fe.

The S values for the pure Fe sample decrease continuously with increasing positron energy after an initial steep rise in S (at $E < 3$ keV), this being attributable to surface effects. This trend corresponds with delocalized positron annihilation, characteristic of well-annealed material [34]. However, the non-irradiated $Fe_{85}Cr_{15}$ specimen shows an almost constant S value, higher than that of the pure Fe one. This result suggests that some vacancy-type defects could be already present in the samples in the non-irradiated state (prior to irradiation). These defects could correspond to dislocations generated by the mechanical deformation occurring during sample preparation.

In the case of the Fe^+ irradiated $Fe_{85}Cr_{15}$ (#3 and #4), Fig. 7 a, it is observed that above 2 keV there is a sharp increase in the S

values, what is indicative of a higher fraction of trapped positrons due to the presence of irradiation-induced open volume defects. The S parameter reaches its maximum value at positron energies between 15 and 20 keV for the sample irradiated in the absence of a magnetic field. These positron energies correspond to mean implantation depths of 390-620 nm, indicating that the radiation damage extends to a depth deeper than that predicted by codes. So, SRIM code shows a maximum in the produced vacancies at about 300 nm (see Fig. 1b), meanwhile SPAS results occur to a depth of 600 nm. At higher positron energies, the S parameter value starts decreasing, however it does not reach the unirradiated value. For the maximum positron energy of 30 keV (that corresponds to a mean implantation depth of ~1.2 μm) a considerable fraction of positrons is still annihilating with irradiation induced defects.

The S parameter values for the Fe^+ irradiated sample (#4) in the presence of B field follow a similar behaviour, although they are slightly lower for positron energies between 10 and 20 keV, that means in the region of expected maximum damage. This would imply that when the samples are irradiated under an applied field either a lower amount of defects was generated or the vacancy clusters created have smaller sizes than in the case of the samples irradiated in absence of a magnetic field.

The effect of the subsequent He^+ irradiation can also be observed in Fig. 7a. As the damage created by the He^+ ions is several orders of magnitude smaller than the damage created by the heavier Fe^+ ions, the S values do not increase anymore. On the contrary, the S parameter measured for samples #7 and #8 decrease with respect to the previous ones in the range 4-20 keV, reaching a local minimum at ~9 keV. This energy correspond to ~170 nm mean positron implantation depth, which coincides with the maximum concentration of He^+ implanted ions predicted by SRIM (200 nm approximately, Fig. 1b). The lowering of the S values result from filling the vacancy clusters already present in the damaged material with He atoms. This increases the rate of positrons annihilating with core electrons, as the W parameter shows (see Fig. 7b). Above 20 keV the He effect disappears completely and the S values coincide with the single Fe^+ irradiated ones indicating that vacancy clusters in the deeper regions remain unaffected by the He^+ ions. As it has been described before, samples sequentially irradiated in the presence of magnetic field show lower values than the samples irradiated in absence of B field. This result further supports that the size or concentration of the vacancy clusters created during the Fe^+ ion irradiation diminishes in the presence of the magnetic field. During the second irradiation the number of injected He^+ ions would remain the same, filling the pre-existent vacancy clusters and decreasing the S values accordingly.

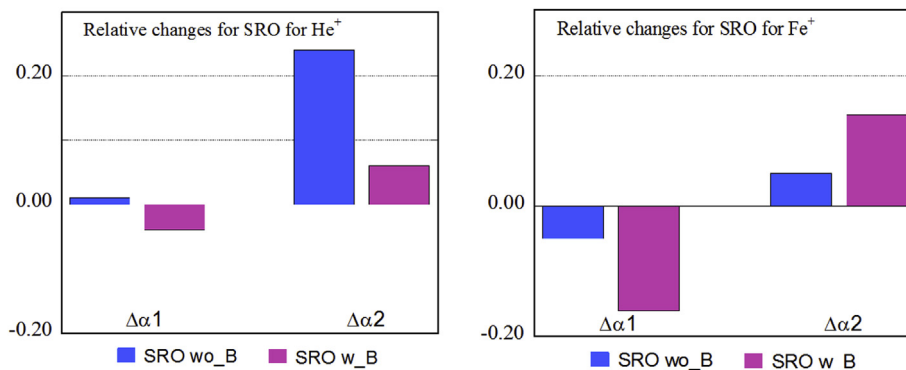The correlation between the S and W parameters for positron

Fig. 6. Differences in the SRO parameters, $\Delta<\alpha_1>$ and $\Delta<\alpha_2>$, between the irradiated samples and the A.R. sample. LHS: for irradiation with He^+, RHS: for irradiation with Fe^+. The source data are taken from Table 4. Note: "wo_B″ are samples irradiated in absence of B and "w_B" irradiated in the presence of B.
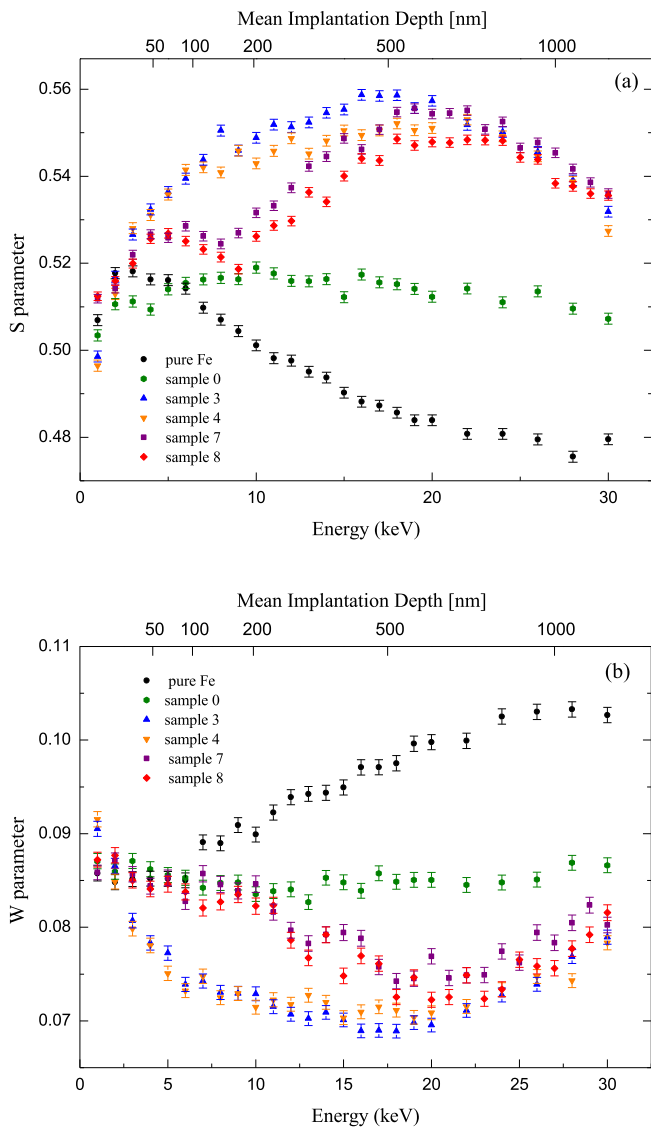
Fig. 7. SPAS line-shape parameters S and W for samples irradiated with Fe+ 22 dpa, w/o_B (#3) and w_B (#4), and sequentially irradiated with with Fe+ 22 dpa and He+ 8000 appm w/o_B (#7) and w_B (#8) with respect to positron energy. Note: "wo_B" are samples irradiated in absence of B and "w_B" irradiated in the presence of B.

energies between 4 and 20 keV is shown in Fig. 8. As it can be observed, the defect-specific S/W plot follows a trend similar to that of both samples irradiated with Fe+ ions and the unirradiated one (dashed line), indicating that there is no significant change in the type and nature of the positron trapping sites present. The S/W plot for the sequentially irradiated samples lies above the previous ones with a similar slope (solid line). This difference, albeit weak, could point to a different kind of positron trap due to the presence of the He-vacancy complexes. The S/W plots for the samples irradiated under the influence of the magnetic field are very similar to the ones obtained for samples irradiated in absence of B for both irradiations; single and sequential, therefore indicating that the presence of magnetic field does not produce any significant change in the type of positron traps generated.

Fig. 9 shows the CDB spectra of both the Fe+ irradiated samples and the unirradiated one normalized to that recorded from annealed pure Fe. The CDB measurements have been performed at positron energies of 17 keV for the irradiated samples and 30 keV

for the non-irradiated material. The CDB spectrum for the unirradiated material shows already the presence of vacancy-type defects. This has been observed by other authors as a result of the sample machining and preparation. As expected, the fraction of positrons annihilating with low-momentum electrons, *i.e.*, $p_L < 3 \times 10^{-3}$ m_0c, in both irradiated samples is much higher than in the non-irradiated one. In all samples a local minimum appears at $p_L \sim 15 \times 10^{-3}$ m_0c, this being much deeper in both irradiated samples due to the presence of the irradiation induced vacancy-type defects. Moreover, the ratio curves for pure Fe are very similar for the two samples along the whole momentum range, irrespective of the presence or not of a magnetic field, indicating that there are not any significant difference in the structure of the vacancy-type defects created by irradiation.

4. Discussion

Irradiation studies of $Fe_{85}Cr_{15}$ samples, at low temperature, have been carried out using independently light and heavy ions and sequentially heavy plus light ions. The influence of an external magnetic field has also been considered. Analysis of the irradiated samples has been done using different techniques, for instance, information on the distribution of Cr and/or vacancies can be obtained from Mössbauer spectroscopy, vacancy-type defect depth profiles by SPAS. In the following paragraphs the results are discussed in detail.

Large differences in damage parameters have been observed between samples irradiated by He+ and Fe+ ions in the case of no external magnetic field. Mössbauer Spectroscopy has revealed differences in the average hyperfine magnetic field ($<\Delta H> = 0.8$ T), see Figs. 2–4. For each ion used to damage the material, the corresponding fitted Mössbauer spectra reveal different configurations of the Cr/vacancies around the probe nuclei (^{57}Fe), especially in the two first neighbouring shells (Fig. 2). The specimens irradiated by light ions, He+ @45 keV, show an increased hyperfine magnetic field, this pointing to a larger clustering in the distribution of the Cr atoms than in the as received or the irradiated samples damaged by Fe+ ions. Moreover, SRO parameters (Fig. 5 or Table 4) point to the formation of Cr clusters as well, in agreement with ref [25] in which a linear increase of the Cr-clustering effect with dose was found. Here, it is hypothesized that the creation of He bubbles could induce clustering of Cr, as suggested from modelling in Ref. [35].

In contrast, the average hyperfine magnetic field shows a clear drop, with respect to the A.R. sample, in samples irradiated by self-ions (Fe+) at low temperature (- 80 °C) to a high dose of 30 dpa (see Fig. 4). Assuming that the vacancy-Cr binding energy is negligible [14], this can result from two possible effects: lower clustering of the Cr atoms and/or an increase of vacancy-type defects since both effects can reduce the hyperfine magnetic field. In this sense, it is seen in Fig. 7 that the samples damaged by Fe+ @1 MeV up to 22 dpa, show high levels of vacancy-type defects, this being in agreement with results in Ref. [34] and with the profiles measured in neutron irradiated Fe-Cr alloys [36]. Moreover, in Fe-Cr alloys with Cr concentrations above 9–10%, since high SRO is an unexpected phenomenum [14,37], our hypothesis points to a competition between, mainly, two terms:

a) clustering of Cr atoms: as an effect arising from of Fe+ irradiation, something that has been also observed in $Fe_{90}Cr_{10}$ irradiated by Fe+ @1 MeV up to 15 dpa [15] and
b) high level of vacancy-type defects as observed by SPAS (Fig. 7).

Both terms will have opposite effect in $<H>$ measused by Mössbauer spectrocopy, where meanwhile the Cr-clusters tend to increase $<H>$, a high level of vacancies tend to reduce $<H>$. It
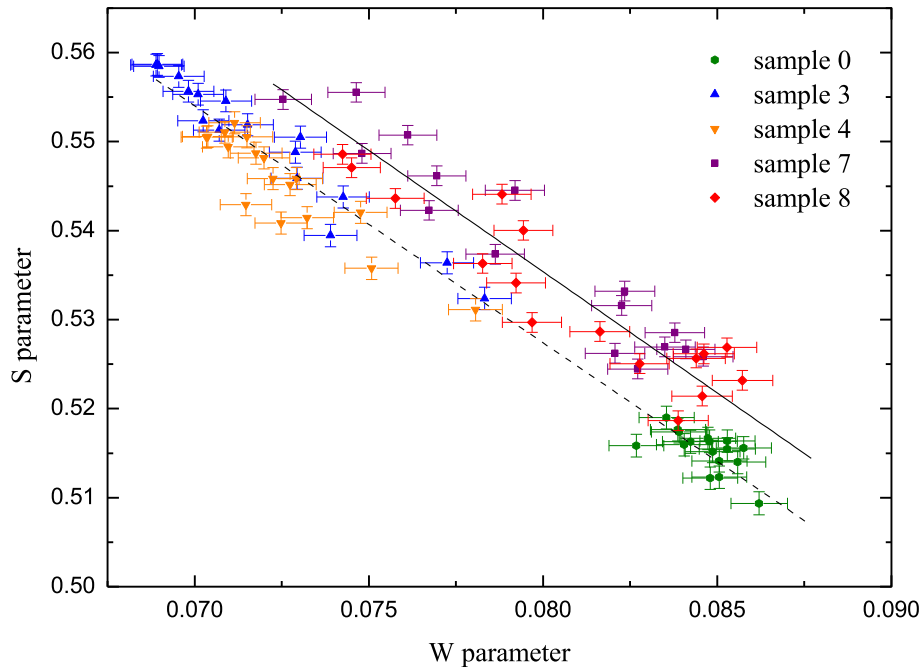
Fig. 8. S-W correlation between different samples, i.e., non-irradiated (#0), Fe$^+$ irradiated at 22 dpa wo_B (#3) and w_B (#4), and sequentially irradiated with with Fe$^+$ 22 dpa and He$^+$ 8000 appm w/o_B (#7) and w_B (#8), measured at incident positron energies in the 4–20 keV range. Note: "wo_B" are samples irradiated in absence of B and "w_B" irradiated in the presence of B.
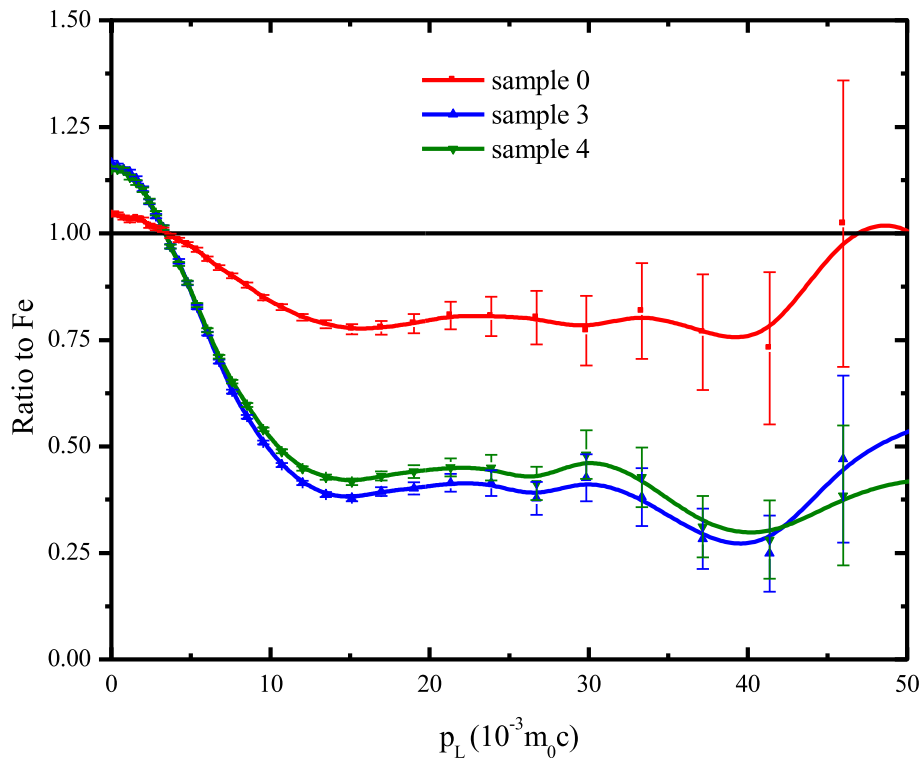

Fig. 9. CDB ratio curves with respect to pure Fe for Fe$_{85}$Cr$_{15}$ non-irradiated (#0) and irradiated with Fe + ions up to 22 dpa, wo_B (#3) and w_B (#4). The CDB spectra were measured at either 30 or 17 keV incident positron energy, respectively. Note: "wo_B" are samples irradiated in absence of B and "w_B" irradiated in the presence of B.

appears that, in the case of samples irradiated by Fe$^+$ at high dose, the vacancy-type defects dominate the effect on the magnitude of hyperfine magnetic field.

In addition, the influence in damage of an external magnetic field has been also studied in this work. The Fe$_{85}$Cr$_{15}$ samples irradiated by Fe$^+$ in the presence of an external magnetic field show small differences as compared with the samples irradiated in the absence of B field. In terms of vacancy profiles, the depth region

between 200 and 600 nm of the samples irradiated in the presence of magnetic field shows a lower vacancy density or smaller size of the vacancy clusters than in the samples irradiated without the influence of B. In the case of the Mössbauer magnitudes, the application of a B field changes the profile of the sextet distributions and, therefore, different atomic configurations may be expected. As a consequence, a difference, with respect to the samples without the presence of B field, appears in the Cr/vacancies distribution, in particular in $<\alpha_{12}>$, i.e., the samples irradiated under the influence of B are more similar to the as received samples, especially in samples irradiated with He^+ ions. The irradiation under an external magnetic field differs much less from the as received material than the samples irradiated in absence of B field in terms of the distribution of the Cr/vacancies, i.e., $<m+n>$ and also it shows small differences in $<H>$ in comparison with the samples irradiated in absence of B. This infers reduced influence in damage when irradiated under B field with respect to the irradiation without its effect. A similar influence in the $<H>$ was previously observed in Mössbauer Spectra of $Fe_{90}Cr_{10}$ [15] irradiated by Fe^+.

SPAS result of sequential irradiation (Fe^+ and He^+) further supports that the size or concentration of the vacancy clusters created during the Fe^+ ion irradiation diminishes in the presence of the magnetic field. During the second irradiation the number of injected He^+ ions would remain the same, filling the pre-existent vacancy clusters and decreasing the S values accordingly. The decrease of the S parameter after helium implantation in samples containing previous defects has already been observed in deformed pure iron [38]. The CDB measurements in the Fe^+ ion irradiated samples confirm the previous results as the ratios for the samples irradiated in absence of B are slightly more pronounced than the samples irradiated under the influence of B. This again would imply that a lower concentration of vacancy-type defects could have been generated in the samples irradiated in the presence of a magnetic field.

The results presented here, although recorded at temperatures and magnetic field strengths lower than those expected for a fusion reactor, highlight the importance of undertaking studies at device relevant conditions (temperatures above 450 °C [39], triple irradiation and magnetic fields of several Teslas) and in particular to evaluate vacancy profiles and chromium mobility due to the defect creation. These experiments are crucial to understand if the magnetic field can play a role in the resulting damage due to neutrons in conditions close to the reactor. Such studies are currently in progress and will be reported in the future.

5. Conclusions

Damage in $Fe_{85}Cr_{15}$ alloy (15% Cr content) when irradiated at low temperature by heavy (Fe^+) and light (He^+) ions, single and sequentially has been studied and additionally, the influence of an external magnetic field (B = 0.4 T) has been also taken into account. The main results are summarysed here:

1. In absence of B field: Our comparison between samples irradiated by He^+ and Fe^+ shows large differences in terms of the distribution of Cr and/or vacancies, taking into account the values of different Mössbauer parameters like the average hyperfine magnetic field ($<\Delta H> = 0.8$ T). That is, samples irradiated by He^+ point to Cr clustering while the specimens irradiated by Fe^+ show a possible clustering of Cr atoms competing with a high level of vacancy-type defects. The profile of vacancies probed here is deeper than that predicted from computer simulations, this being a consequence of Fe^+ damage. On the other hand, in samples with sequential irradiation, Fe^+ and then He^+, the vacancy-type defect profiles show a clear

reduction in the depth where He^+ is implanted pointing to a filling of the vacancy clusters by He atoms.

2. Under the influence of B: studies of the influence of an external magnetic field (B = 0.4 T) on defects show small but not insignificant differences in the magnitudes studied here for the $Fe_{85}Cr_{15}$ alloy. Mössbauer spectra point to less clustering for a sample damaged by He^+ (being closer to the A.R.) compared to irradiation without B. SPAS points to slightly lower values of vacancy-type defects over a large region when a sample is damaged by self-ions (Fe^+, high dose) or by sequential irradiation: Fe^+ and He^+ (again compared to irradiation without B). SPAS results further support the conclusion that the size or concentration of the vacancy clusters created during the Fe^+ ion irradiation diminishes in the presence of B.

The detailed studies carried out here indicate that an external magnetic field can be a parameter to take into account in damage studies that needs more experimental work and modelling efforts for clarification. Experiments with higher B and higher sample temperature are currently in progress in order to elucidate if external magnetic fields are a key parameter in the structural materials damage.

References

[1] D. Stork, S.J. Zinkle, Nucl. Fusion 57 (2017), 092001.
[2] E.A. Little, D.A. Stow, J. Nucl. Mater. 87 (11—24) (1979) 25—39.
[3] F.A. Garner, M.B. Toloczko, et al., J. Nucl. Mater. 276 (2000) 123—142.
[4] A. Bhattacharya, E. Meslin, et al., Acta Mater. 108 (2016) 241—251.
[5] M. Wall, Temper Embrittlement in 9% Cr Steels, Ph.D. Thesis, Imperial College, University of London, 1985.
[6] R. Lagneborg, et al., Trans. Amer. Soc. Metals 60 (1967) 67—78.
[7] P.J. Groebner, Metall. Trans. 4 (1973) 251—260.
[8] J.L. Boutard, A. Alamo, R. Lindau, M. Rieth, Compt. Rendus Phys. 9 (2008) 287—302.
[9] R.L. Klueh, D.R. Harries, High-chromium Ferritic and Martensitic Steels for Nuclear Applications, ASTM International, 2001. ISBN 0-803102090-7.
[10] S.J. Zinkle, Phys. Plasmas 12 (2005), 058101.
[11] O. Motojima, Nucl. Fusion 55 (2015) 104023.
[12] D. Stork, P. Agostini, et al., J. Nucl. Mater. 455 (2014) 277—291.
[13] T. Seletskaia, Y. Osetsky, et al., Phys. Rev. Lett. 94 (2005), 046403.
[14] L. Malerba, A. Caro, et al., J. Nucl. Mater. 382 (2008) 112—125.
[15] F.J. Sánchez, I. García-Cortés, et al., Nucl. Mat. Energy. 9 (2016) 476—479.
[16] R.S. Averback, R. Benedek, K.L. Merkle, J. Nucl. Mater. 75 (1978) 162.
[17] H. Ullmaier, Ann. Chim. Fr. Sci. Mat. 9 (1984) 263.
[18] D. Jiménez-Rey, F. Mota, et al., J. Nucl. Mater. 417 (2011) 1352—1355.
[19] J. Le Coze, Procurement of Pure Fe Metal and Fe-Based Alloys with Controlled Chemical Alloying Element Contents and Microstructure. Final Report on Model Alloy Preparation, Armines Ecole Nationale Superieure des Mines, Saint Etienne, France, 2007.
[20] J.F. Ziegler, J.P. Boersack, U. Littmark, The Stopping and Ranges of Ions in Solids, Pergamon, New York, 1985 see also the SRIM web page, http://www.srim.org.
[21] A. Climent-Font, F. Pászti, et al., Nucl. Instrum. Methods Phys. Res. Sect. B Beam Interact. Mater. Atoms 219—220 (2004) 400—404.
[22] Laboratorio Nacional de Fusión, CIEMAT, Ion Implanter, 2017. http://www.fusion.ciemat.es/competitive-access-to-facilities/ion-implanter/.

[23] B. Gómez-Ferrer, I. García-Cortés, et al., Phys. Rev. B 90 (2014) 220102 (R).
[24] S.M. Dubiel, J. Żukrowski, Acta Mater. 61 (2013) 6207–6212.
[25] S.M. Dubiel, J. Cieslak, et al., J. Nucl. Mater. 434 (2013) 235–239.
[26] S.S. Huang, S. Kitao, et al., J. Nucl. Mater. 456 (2015) 266–271.
[27] J.R. Gancedo, M. Gracia, et al., Hyperfine Interact. 66 (1991) 83–93.
[28] Heinz Maier-Leibnitz Zentrum, NEPOMUC: neutron induced positron source Munich, J. Large-scale Res. Facil. 1 (2015) A22 (2015).
[29] Heinz Maier-Leibnitz Zentrum, CDBS: coincident Doppler-broadening spectrometer, J. Large-scale Res. Facil. 1 (2015a) A23 (2015a).
[30] P. Asoka-Kumar, M. Alatalo, et al., Phys. Rev. Lett. 77 (1996) 2097–2100.
[31] S.M. Dubiel, J. Cieslak, et al., Phys. Rev. B 83 (2011) 180202 (R).
[32] M. Gracia, J.F. Marco, et al., Surf. Interface Anal. 29 (2000) 82.
[33] E. Murad, J.H. Jonhston, et al., Iron oxides and oxyhydroxides, in: G.J. Long (Ed.), Mössbauer Spectroscopy Applied to Inorganic Chemistry, vol. 2, Plenum Press, New York, 1987, pp. 507–582.
[34] W. Anwand, T. Leguey, et al., Fe$^+$ implantation induced damage in oxide dispersion strengthened steels investigated by Doppler broadening spectroscopy, Defect Diffus. Forum 373 (2016) 113–116. ISSN: 1662-9507.
[35] E. Martínez, Ch Fu, Phys. Rev. B 84 (2011), 014203.
[36] M. Lambrecht, L. Malerba, Acta Mater. 59 (2011) 6547–6555.
[37] I. Mirebeau, M. Hennion, G. Parette, Phys. Rev. Lett. 53 (1984) 687.
[38] Y.H. Gong, X.Z. Cao, et al., J. Nucl. Mater. 482 (2016) 93–98.
[39] M. Stepanovic, M. Auger, et al., Mater. Char. 136 (2018) 318–330.